Impact of the coordinated nitrogen atom on the electrocatalytic water oxidation properties of copper complexes with pentadentate ligands

Zhichao Qi,[a] Jinlin Hu,[a] Zhijun Ruan,[a] Yanmei Chen,[a] Yanbo Qu,[*a] Xiangming Liang,[*b] Junqi Lin[*a]

[a] Hubei Key Laboratory of Processing and Application of Catalytic Materials, College of Chemistry and Chemical Engineering, Huanggang Normal University, Huanggang, 438000 China.

[b] School of Basic Medical Sciences, Ningxia Medical University, Yinchuan, 750004, China. Email: pony029@126.com, liangxm6@163.com, linjunqi@hgnu.edu.cn

Table 1 Crystal data and structure refinement for $[Cu(tetren)](ClO_4)_2$.

Complex parameters	$[Cu(tetren)](ClO_4)_2$
Empirical formula	$C_8H_{20}Cl_2CuN_5O_8$
Formula weight	448.73
Temperature / K	276.0
Wavelength / Å	0.71073
Crystal system	monoclinic
Space group	Cc

a / Å	8.3439(14)
b / Å	15.187(3)
c / Å	14.026(3)
α / deg	90
β / deg	98.286(4)
γ / deg	90
Volume / Å^3	1758.9(5)
Z	4
Calculated density / g cm^{-3}	1.695
Absorption coefficient	1.592
F(000)	920
Crystal size / mm	0.24 × 0.35 × 0.41 mm^3
θ range / deg	2.682 to 20.068
Index ranges	-9 ≤ h ≤ 9, -18 ≤ k ≤ 18, -16 ≤ l ≤ 16
Reflections collected	12490
Independent reflections	3124 [R(int) = 0.1276]
Completeness to theta = 24.792°	99.9 %
Absorption correction	Semi-empirical from equivalents
Max. and min. transmission	0.7451 and 0.6188
Data / restraints / parameters	3124 / 2 / 226
Goodness-of-fit on F^2	1.035
Final R indices [I>=2σ (I)]	R_1 = 0.0627, wR_2 = 0.1369
R indices (all data)	R_1 = 0.1179, wR_2 = 0.1641
Largest diff. peak and hole / e Å^{-3}	0.33/-0.36

$R_1 = \Sigma||F_o| - |F_c||/\Sigma|F_o|$, $wR_2 = [\Sigma(|Fo|^2 - |Fc|^2)^2/\Sigma(Fo_2)]^{1/2}$

Table 2 Crystal data and structure refinement for [Cu(pydien)](ClO$_4$)$_2$.

Complex parameters	[Cu(pydien)](ClO$_4$)$_2$ (**2**)
Empirical formula	$C_{16}H_{23}Cl_2CuN_5O_8$
Formula weight	547.83
Temperature / K	293(2)
Wavelength / Å	0.71073
Crystal system	Orthorhombic

Space group	Pbca
a / Å	14.9870(3)
b / Å	9.9557(3)
c / Å	29.6358(7)
α / deg	90
β / deg	90
γ / deg	90
Volume / Å^3	4421.84(19)
Z	8
Calculated density / g cm^{-3}	1.646
Absorption coefficient	1.283
F(000)	2248
Crystal size / mm	0.27 × 0.21 × 0.19 mm^3
θ range / deg	1.933 to 24.792
Index ranges	-17≤h≤16, -11≤k≤11, -34≤l≤34
Reflections collected	55423
Independent reflections	3797 [R(int) = 0.0710]
Completeness to theta = 24.792°	99.9 %
Absorption correction	Semi-empirical from equivalents
Max. and min. transmission	0.7451 and 0.6188
Data / restraints / parameters	3797 / 20 / 313
Goodness-of-fit on F^2	1.088
Final R indices [I>=2σ (I)]	R_1 = 0.0830, wR_2 = 0.2644
R indices (all data)	R_1 = 0.1044, wR_2 = 0.2947
Largest diff. peak and hole / e Å^{-3}	1.580 and -0.966 e.Å^{-3}

$R_1 = \Sigma||F_o| - |F_c||/\Sigma|F_o|$, $wR_2 = [\Sigma(|Fo|^2 - |Fc|^2)^2/\Sigma(Fo_2)]^{1/2}$

Table S3 Selected bond lengths (Å) and angles (deg) for complex **1** and **2**.

Complex	**1**	**2**
Bond length (Å)		
Cu–N1	2.114(13)	2.029(6)
Cu–N2	1.995(17)	1.966(8)
Cu–N3	2.038(12)	2.005(7)
Cu–N4	2.014(16)	2.155(6)

Cu–N5	2.061(13)	2.108(5)
Bond angles (deg)		
N1–Cu–N2	84.8(6)	83.1(2)
N1–Cu–N3	115.4(6)	162.3(3)
N1–Cu–N4	104.8(6)	106.8(2)
N1–Cu–N5	108.6(6)	96.98(19)
N2–Cu–N3	84.4(6)	79.2(3)
N2–Cu–N4	167.9(7)	129.4(4)
N2–Cu–N5	99.2(6)	149.4(4)
N3–Cu–N4	84.8(7)	84.7(3)
N3–Cu–N5	136.0(6)	98.2(3)
N4–Cu–N5	84.8(6)	80.1(2)

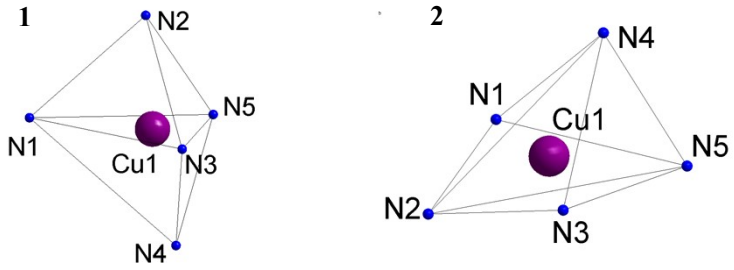

Fig. S1 The geometry configuration of complex **1** (left) and complex **2** (right).

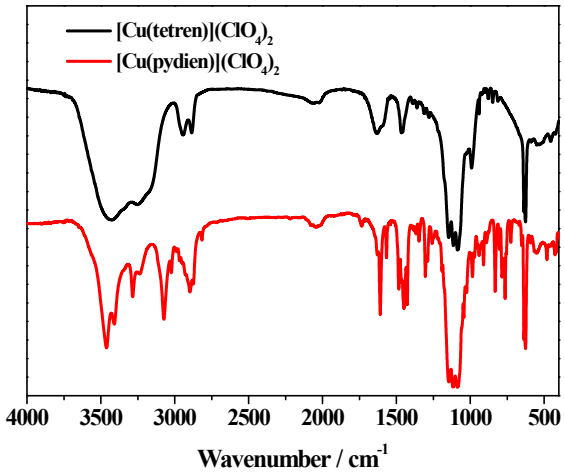

Fig. S2 Infrared spectrum of complex **1** and complex **2**.

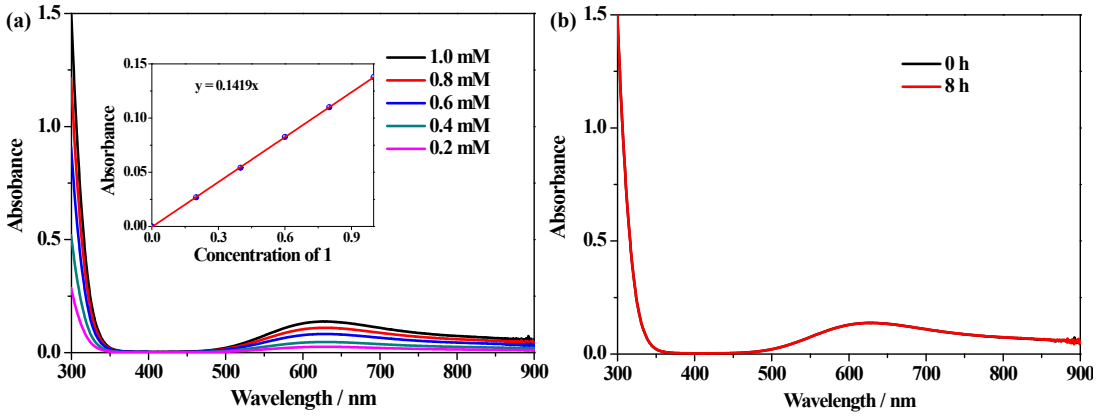

Fig. S3 (a) Concentration-dependent UV-vis absorption spectra of **1** in 0.1 M PBS at pH 8.0; (b) Time-dependent UV-vis absorption spectra of 1 mM of **1** in 0.1 M PBS at pH 8.0.

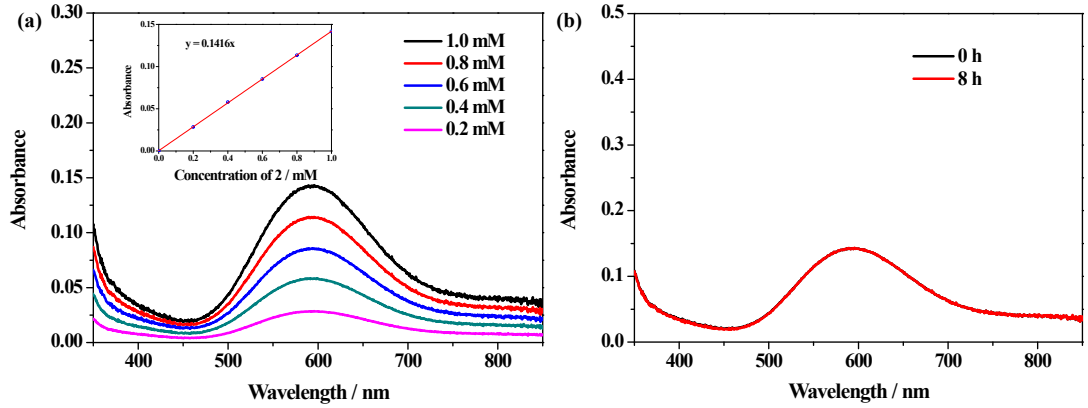

Fig. S4 (a) Concentration-dependent UV-vis absorption spectra of **2** in 0.1 M PBS at pH 8.0; (b) Time-dependent UV-vis absorption spectra of 1 mM of **2** in 0.1 M PBS at pH 8.0.

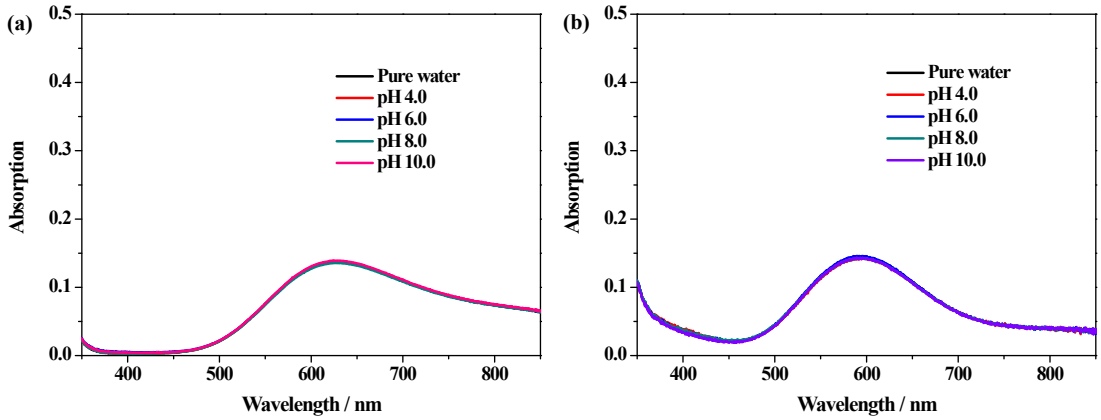

Fig. S5 UV-vis absorption spectra of **1** (a) and **2** (b) in pure water and 0.1 M PBS at various pH value.

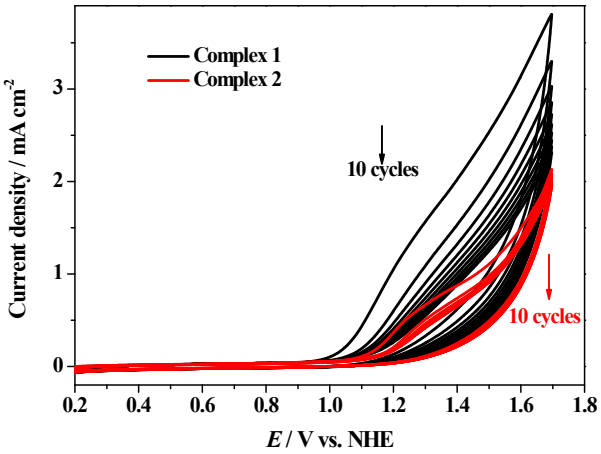

Fig. S6 Consecutive CV cyclic scan curves of 1 mM of **1** and **2** in 0.1 M PBS at pH 8.0, scan rate = 100 mV/s.

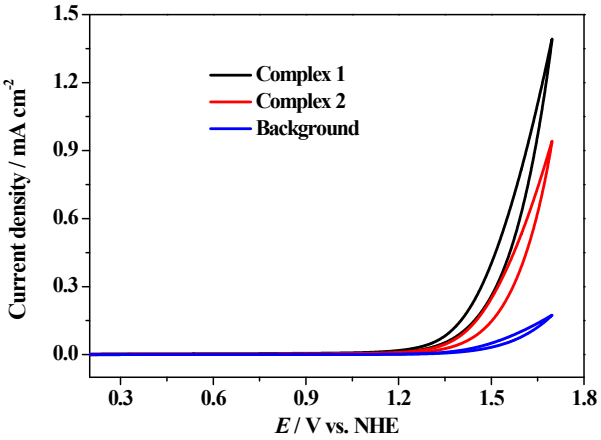

Fig. S7 CV tests of **1** and **2** in 0.1 M PBS at pH 8.0 with scan rates = 100 mV/s, ITO electrode was used as working electrode.

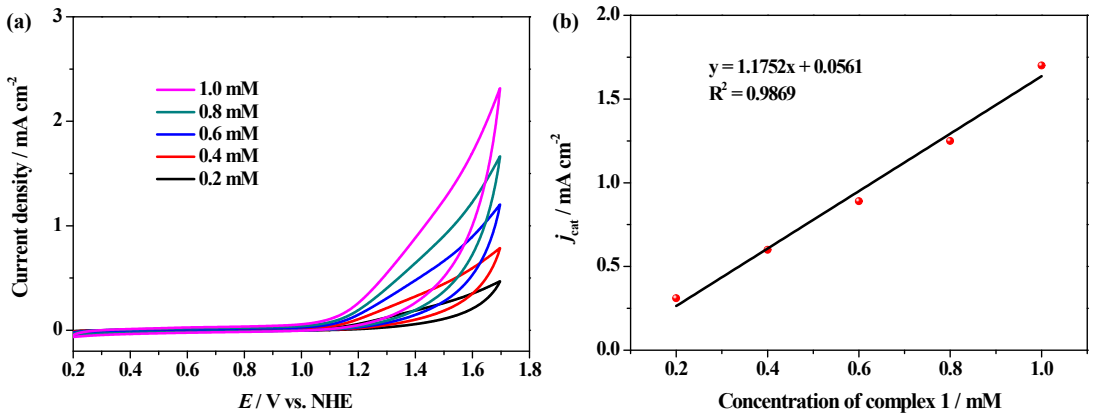

Fig. S8 CV of various concentration of **1** at pH 8.0 with scan rate of 100 mV / s (a) and the dependence of catalytic current density at 1.60 V vs. NHE on the concentration of **1** (b).

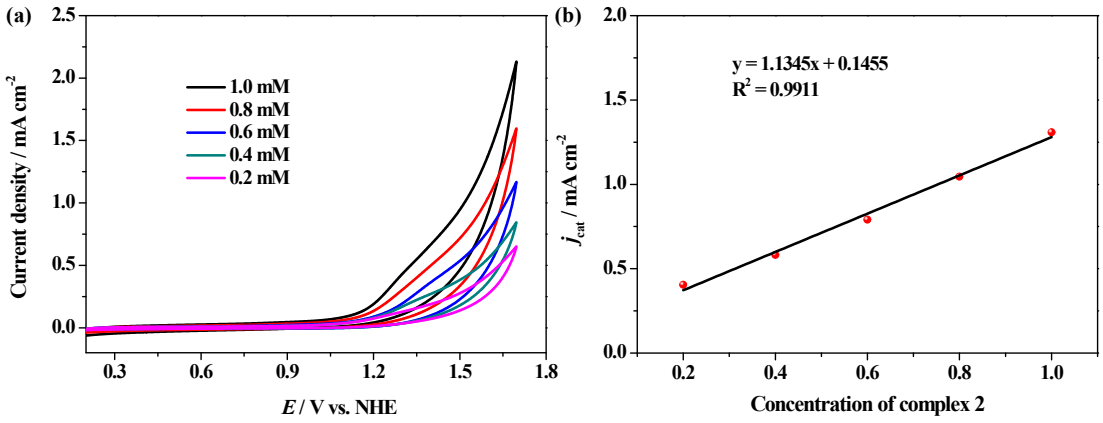

Fig. S9 CV of various concentration of **2** at pH 8.0 with scan rate of 100 mV / s (a) and the dependence of catalytic current density at 1.60 V vs. NHE on the concentration of **2** (b).

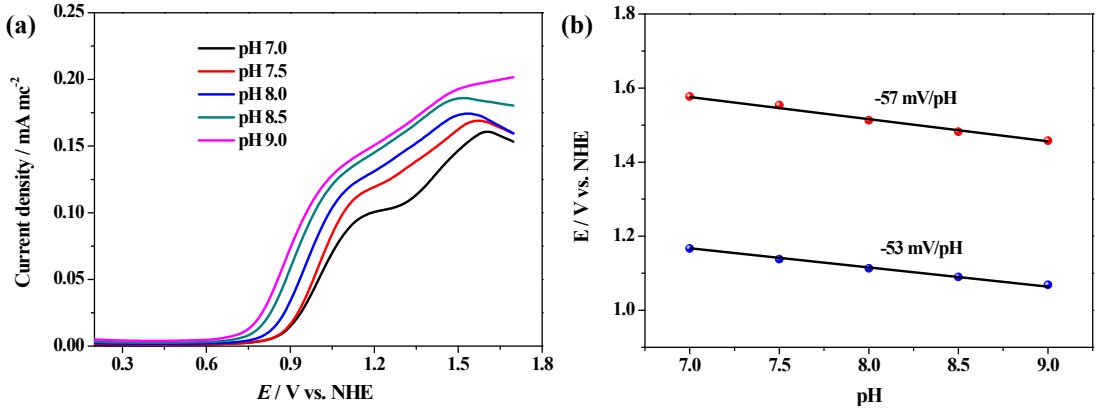

Fig. S10 DPV test of 1 mM **1** in 0.1 M PBS at various pH values (a) and the relationship between the potential of each redox couple of **1** and the pH of electrolyte (b).

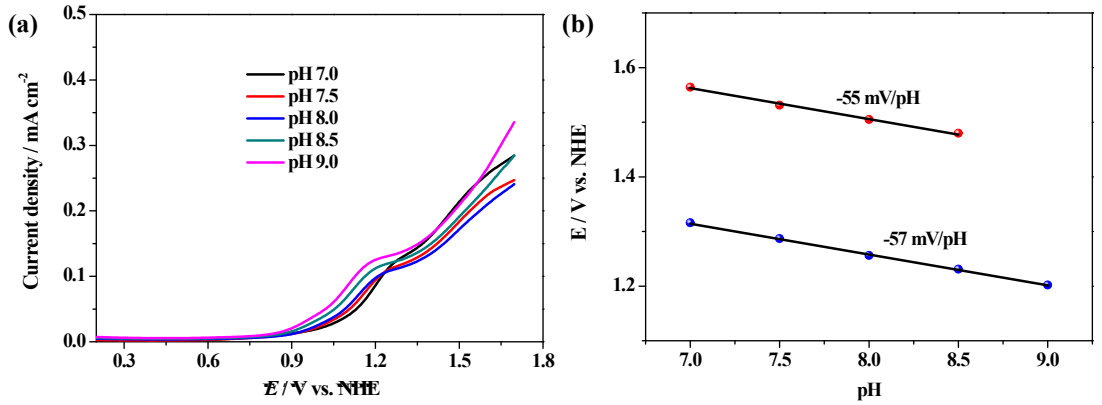

Fig. S11 DPV test of 1 mM **2** in 0.1 M PBS at various pH values (a) and the relationship between the potential of each redox couple of **2** and the pH of electrolyte (b).

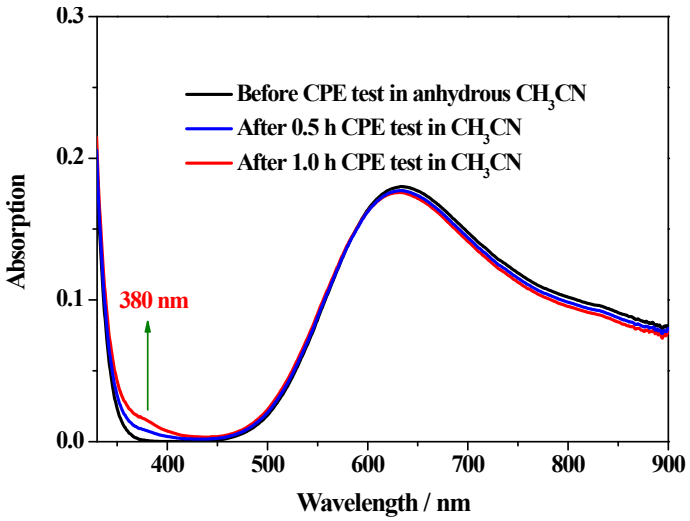

Fig. S12 UV-vis absorbance of 1mM of **1** before and after CPE test at 1.15 V vs. Fc/Fc^{+}, anhydrous CH_3CN containing 0.1 M tetrabutylammonium hexafluorophosphate as electrolyte.

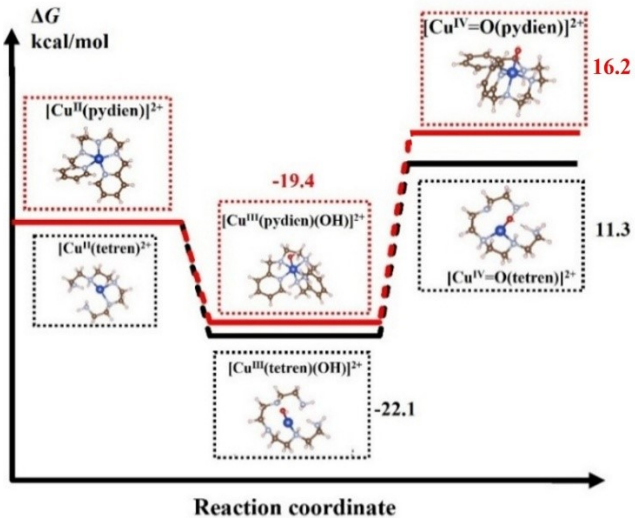

Fig. S13 Relative free energy (ΔG) diagram of the oxidation process of **1** and **2**. DFT calculations were conducted through the Vienna ab initio Simulation Package (VASP) with the projector augment wave method.[S1–S2] Generalized gradient approximation of the Perdew-Burke-Ernzerhof (PBE) functional was used as the exchange-correlation functional.[S3] The Brillouin zone was sampled with 2 × 2 × 1 K points for surface calculation. The cutoff energy was set as 500 eV, and structure relaxation was performed until the convergence criteria of energy and force reached 1×10^{-5} eV and 0.02 eV $Å^{-1}$, respectively. A vacuum layer of 15 Å was constructed to eliminate interactions between periodic structures of surface models. The van der Waals (vdW) interaction was amended by the zero damping DFT-D3 method of

Grimme.[S4] The Gibbs free energy was calculated as ΔG = ΔE + ΔEZPE −TΔS, where the ΔE, ΔEZPE, and ΔS are electronic energy, zero-point energy, and entropy difference between products and reactants. The zero-point energies of isolated and absorbed intermediate products were calculated from the frequency analysis. The vibrational frequencies and entropies of molecules in the gas phase were obtained from the National Institute of Standards and Technology (NIST) database.[S5–S6]

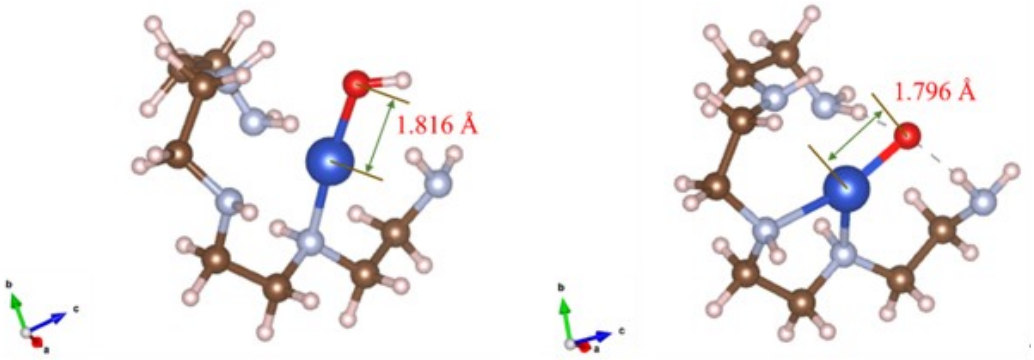

Fig. S14 The calculated Cu–O bond length in the Cu(III)–OH species (left) and Cu(III)–oxyl radical species (right).

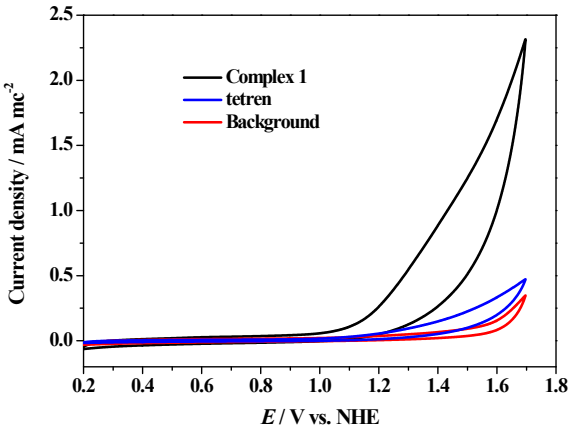

Fig. S15 CV tests of 1 mM of **1** and the ligand tetraethylenepentamine in 0.1 M PBS at pH 8.0 with scan rates = 100 mV / s, GC electrode was used as working electrode.

Fig. S16 Picture of the two-compartment electrochemical cell used for CPE experiments; 0.1 M PBS (pH 8.0) containing 1 mM of **1** was used as electrolyte and potential was controlled at 1.60 V vs. NHE.

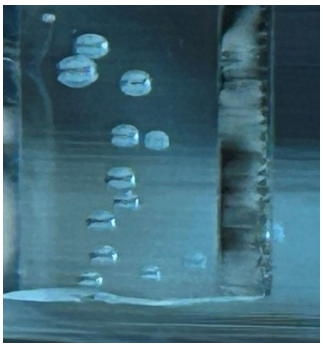

Fig. S17 The oxygen bubbles generated on the surface of ITO electrode during CPE test of 1.

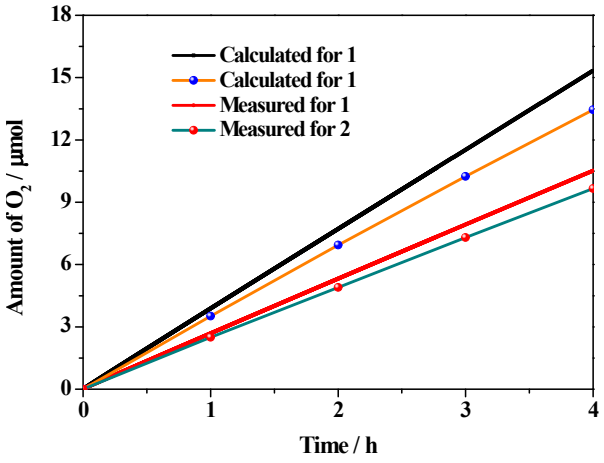

Fig. S18 Faraday efficiency of CPE test of **1** and **2** at 1.60 V vs. NHE, 0.1 M PBS at pH 8.0 was used as electrolyte in a H-shape two-compartment cell.

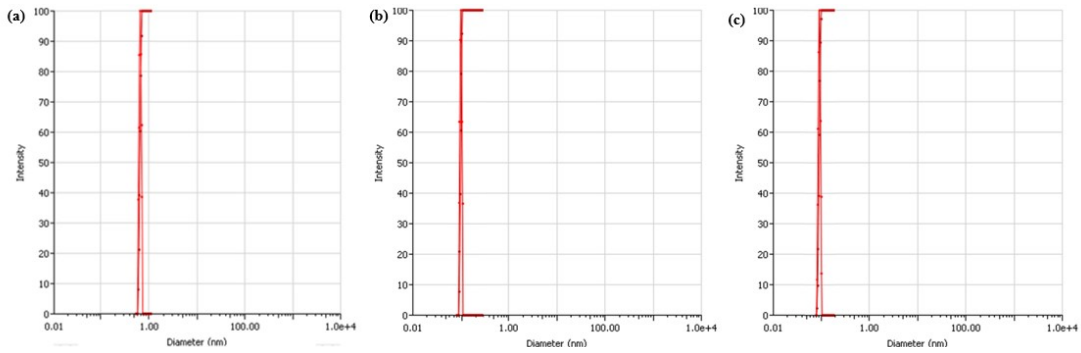

Fig. S19 DLS measurement of fresh PBS (a); DLS measurement of PBS after 4 h CPE test of **1** (b) and **2** (c). Signal below 1 nm is ascribed to the background signal of true solution.

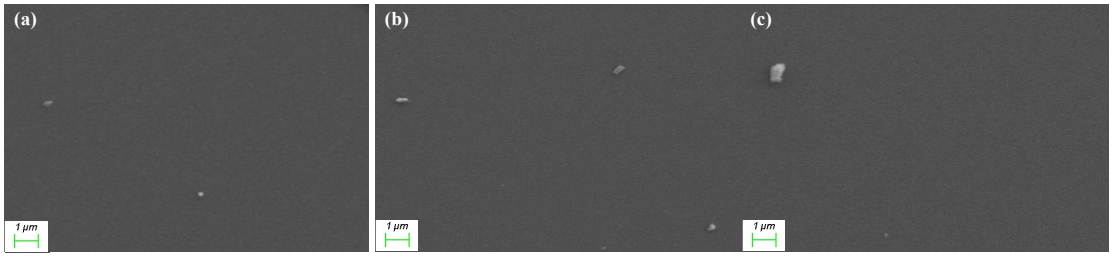

Fig. S20 The SEM images of the clean ITO electrode (a) and the ITO electrode used for electrolysis test of **1** (b) and **2** (c).

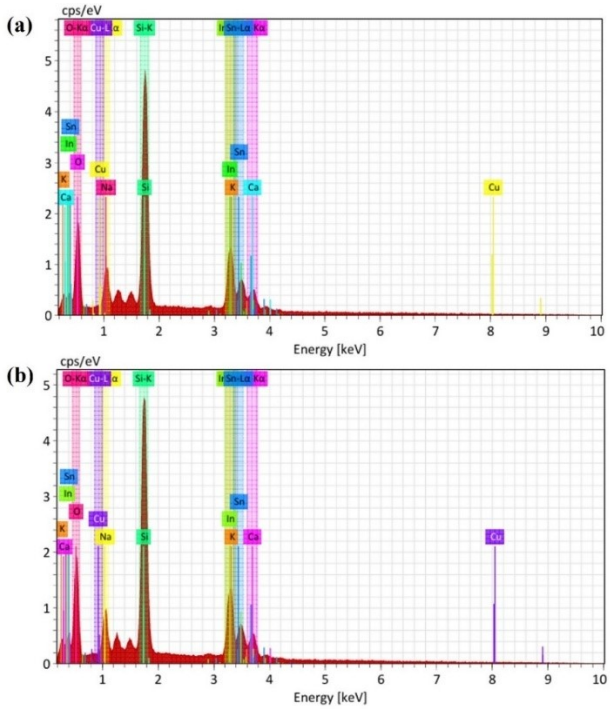

Fig. S21 EDS analysis results of the surface of ITO electrode after 4 h CPE experiments of **1** (a) and **2** (b) in 0.1 M PBS at pH 8.0.

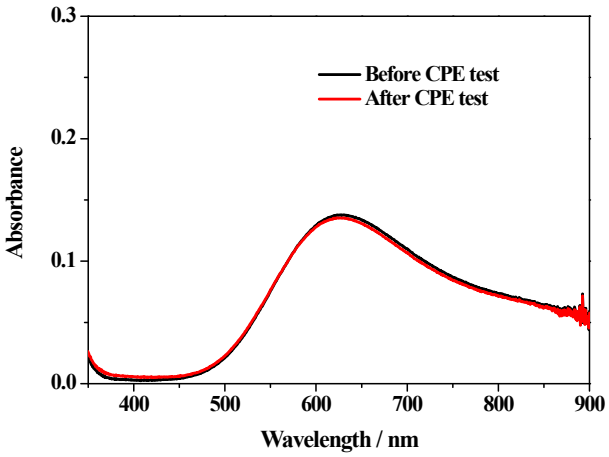

Fig. S22 UV-vis absorbance spectra of 1 mM of **1** before and after 4 h CPE test in the H-shape two-compartment cell with 0.1 M PBS at pH 8.0 as electrolyte.

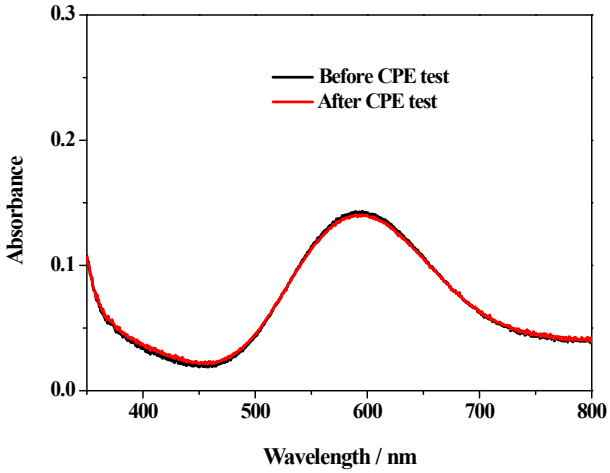

Fig. S23 UV-vis absorbance spectra of 1 mM of **2** before and after 4 h CPE test in the H-shape two-compartment cell with 0.1 M PBS at pH 8.0 as electrolyte.

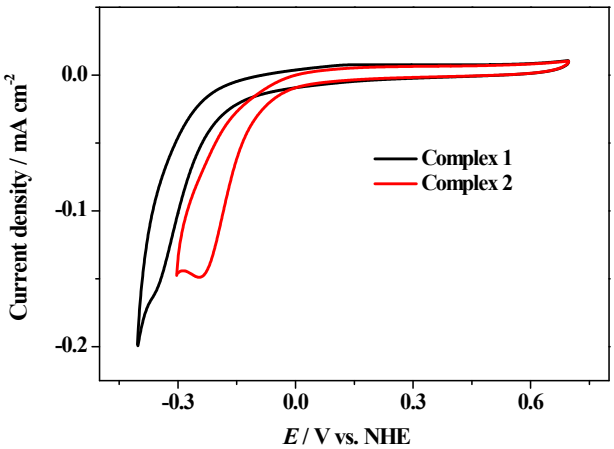

Fig. S24 The Cu^{I}/Cu^{II} couple of **1** and **2** in 0.1 M PBS at pH 8.0, scan rate = 100 mV/s.

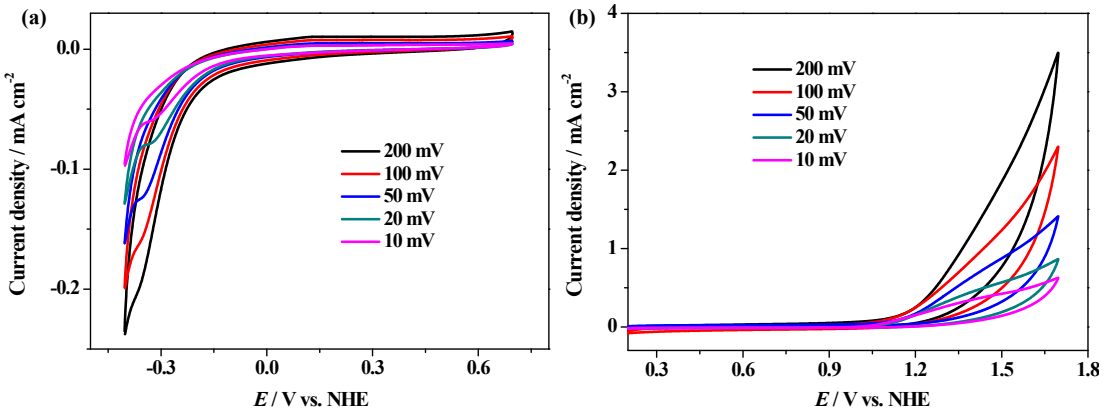

Fig. S25 Cu^{I}/Cu^{II} redox couple of 1.0 mM of **1** with various scan rate (a) and CV of 1.0 mM of **1** in 0.1 M PBSs with scan rate varying from 10 to 200 mV s^{-1} (b).

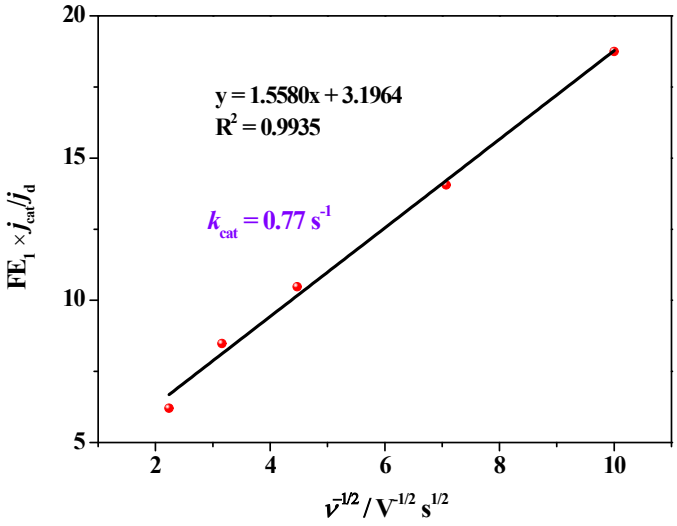

Fig. S26 Plots of the ratio of $FE_1 \times j_{cat}$ to j_d of **1** versus the reciprocal of square root of scan rate.

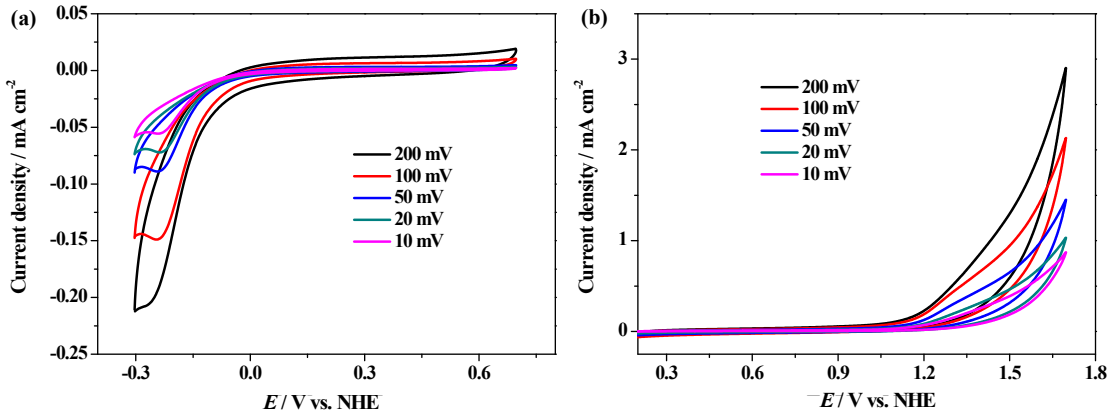

Fig. S27 Cu^{I}/Cu^{II} redox couple of 1.0 mM of **2** with various scan rate (a) and CV of 1.0 mM of **2** in 0.1 M PBSs with scan rate varying from 10 to 200 mV s^{-1} (b).

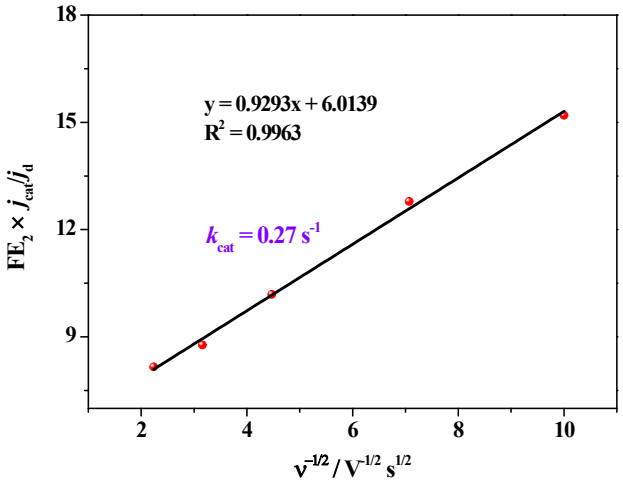

Fig. S28 Plots of the ratio of $FE_2 \times j_{cat}$ to j_d of **2** versus the reciprocal of square root of scan rate.

Table S4 Onset overpotential and TOF value of **1** and some reported Cu based molecular WOC

Catalyst	pH	TOF /s^{-1}	η/mV [a]	Ref.
$[Cu_2(BPMAN)(\mu\text{-}OH)]^{3+}$	7.0	0.6	800	S7
$[Cu_2(TPMAN)(\mu\text{-}OH)(H_2O)]^{3+}$	7.0	0.78	780	S8
$[Cu_3(pda)_3(^t BuPO_3)]$	7.0	0.82	800	S9
$[Cu(mpydien)]^{2+}$	7.0	0.04	640	S10
$[Cu(en)_2(OH_2)_2]^{2+}$	8.0	0.4	440	S11
$[Cu(F_3TPA)]^{2+}$	8.5	0.38	610	S12
$[Cu(dmabpy)]^{2+}$	9.0	0.11	600	S13
$[Cu(mabpy)]^{2+}$	9.0	0.06	870	S13
$[Cu(N_2Py_3)]^{2+}$	11.0	0.81	831	S14
$[Cu(H_2L)(OH)_2]$	12.4	0.4	640	S15
$[Cu(pyalk)_2]$	12.5	0.7	550	S16
$[Cu^{II}(L)]^{2+}$	12.9	0.12	830	S17
1	8.0	0.77	521	This work
2	8.0	0.27	531	This work

[a] η = onset overpotential

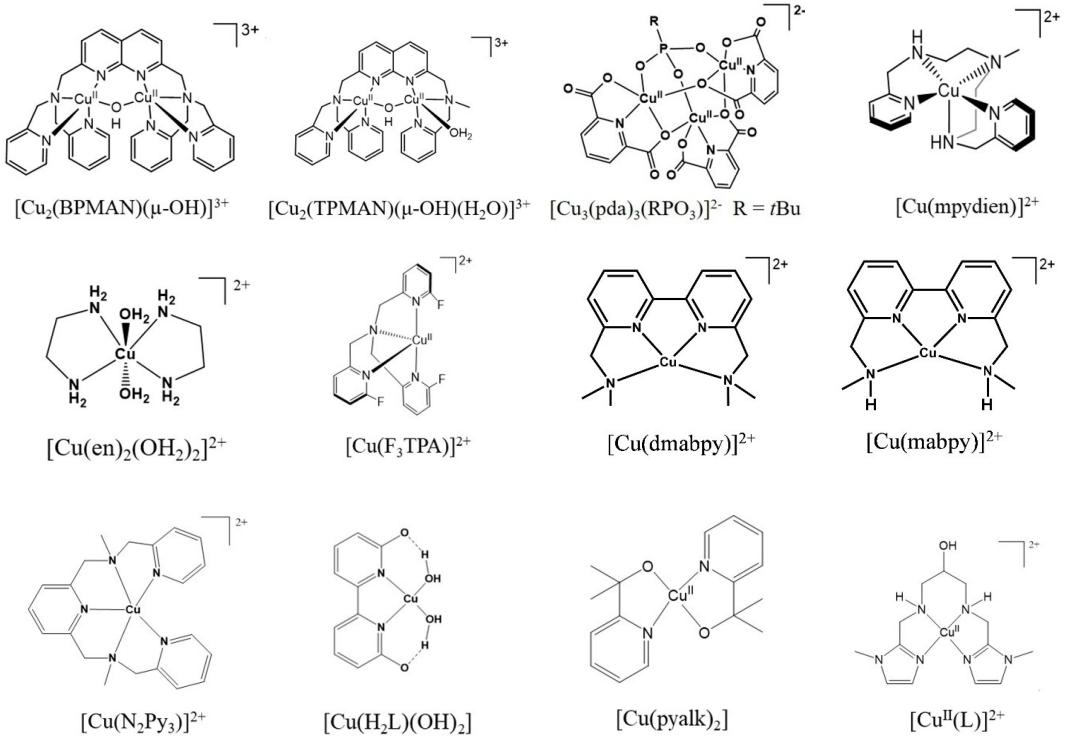

References

1 G. Kresse and D. Joubert, *Phys. Rev. B*, 1999, **59**, 1758–1775.

2 P. E. Blöchl, *Phys. Rev. B*, 1994, **50**, 17953–17979.

3 J. P. Perdew, K. Burke and M. Ernzerhof, *Phys. Rev. Lett.*, 1996, **77**, 3865–3868.

4 S. Grimme, S. Ehrlich and L. Goerigk, *J. Comput. Chem.*, 2011, **32**, 1456–1465.

5 J. K. Nørskov, J. Rossmeisl, A. Logadottir, L. Lindqvist, J. R. Kitchin, T. Bligaard and H. Jónsson, *J. Phys. Chem. B*, 2004, **108**, 17886–17892.

6 J. K. Nørskov, T. Bligaard, A. Logadottir, J. R. Kitchin, J. G. Chen, S. Pandelov and U. Stimming, *J. Electrochem. Soc.*, 2005, **152**, J23.

7 X.-J. Su, M. Gao, L. Jiao, R.-Z. Liao, P. E. M. Siegbahn, J.-P. Cheng and M.-T. Zhang, *Angew. Chem., Int. Ed.*, 2015, **54**, 4909−4914.

8 Q.-Q. Hu, X.-J. Su and M.-T. Zhang, *Inorg. Chem.*, 2018, **57**, 10481–10484.

9 J.-M. Wang, Y.-R. Liu, X.-Y. Mao, N.-N. Shi, X. Zhang, H.-S. Wang, Y.-H. Fan and M. Wang, *Chem.−Asian J.*, 2019, **14**, 2685−2693.

10 24 J. Lin, N. Wang, X. Chen, X. Yang, L. Hong, Z. Ruan, H. Ye, Y. Chen and X. Liang, *Sustainable Energy Fuels*, 2022, **6**, 1312−1318.

11 C. Lu, J. Du, X. J. Su, M. T. Zhang, X. Xu, T. J. Meyer and Z. Chen, *ACS Catal.*,

2016, **6**, 77–83.

12 R.-J. Xiang, H.-Y. Wang, Z.-J. Xin, C.-B. Li, Y.-X. Lu, X.-W. Gao, H.-M. Sun and R. Cao, *Chem. Eur. J.*, 2016, **22**, 1602–1607.

13 J. Wang, Y. Ping, Y. Chen, S. Liu, J. Dong, Z. Ruan, X. Liang and J. Lin, *Dalton Trans.*, 2024, **53**, 5222–5229.

14 Z. Xu, Z. Zheng, Q. Chen, J. Wang, K. Yu, X. Xia, J. Shen and Q. Zhang, *Dalton Trans.*, 2021, **50**, 10888–10895.

15 T. Zhang, C. Wang, S. Liu, J. L. Wang and W. Lin, *J. Am. Chem. Soc.*, 2014, **136**, 273–281.

16 K. J. Fisher, K. L. Materna, B. Q. Mercado, R. H. Crabtree and G. W. Brudvig, *ACS Catal.*, 2017, **7**, 3384–3387.

17 S. Nestke, E. Ronge and I. Siewert, *Dalton Trans.*, 2018, **47**, 10737–10741.